Valence band structure and electron transport properties in rhombic triacontahedron and Mackay icosahedral types of Al-Mg-Pd and other quasi-crystals

1994 J. Phys.: Condens. Matter 6 7335

(http://iopscience.iop.org/0953-8984/6/36/016)

J. Phys.: Condens. Matter 6 (1994) 7335–7350. Printed in the UK

Valence band structure and electron transport properties in rhombic triacontahedron and Mackay icosahedral types of Al–Mg–Pd and other quasi-crystals

U Mizutani†, Y Yamada†, T Takeuchi†, K Hashimoto†, E Belin‡, A Sadoc§||, T Yamauchi¶ and T Matsuda¶

† Department of Crystalline Materials Science, Nagoya University, Furo-cho, Chikusa-ku, Nagoya 464-01 Japan

‡ Laboratoire de Chimie Physique Matiere et Rayonnement (Unité de Recherche associée au CNRS and GDR5), 11 rue Pierre et Marie Curie, 75231 Paris Cédex 05, France

§ Laboratoire pour l'Utilisation au Rayonnement Electromagnétique (CNRS, CEA, MENC and GDR5), Université Paris-Sud, 91405 Orsay Cédex, France

|| LPMS, 49 avenue des Genottes, BP 8428, 95806 Cergy-Pontoise Cédex, France

¶ Department of Materials Science, Aichi University of Education, Kariya-shi, Aichi-ken, 448 Japan

Received 23 February 1994, in final form 26 April 1994

Abstract. The valence band structure of both rhombic triacontahedron (RT) and Mackay icosahedron (MI) types of quasi-crystal (QC) is studied by means of x-ray photoemission spectroscopy and the Al K and Pd L$\beta_{2,15}$ soft x-ray spectroscopy techniques. Information about the density of states at the Fermi level E_F is supplemented by the data on the electronic specific-heat coefficient. The Hall coefficient is also studied. The Al–Mg–Pd, Al–Mg–Zn and Al–Mg–Cu QCs are selected as representative of the RT-type QCs and Al–Mg–Pd, Al–Ru–Cu and Al–Re–Pd as representative of the MI-type QCs. The valence band structure of the RT-type QCs is characterized by a narrow d band in the middle of the valence band and a quasi-free-electron-like smooth density of states in the vicinity of E_F. On the other hand, the d states of the transition-metal elements are more widely spread in the MI-type QCs. The depletion minimum in the Al 3p electron distribution occurs at the binding energies 3–5 eV owing to the interaction with the d states of the late-transition-metal elements. The presence of the pseudo-gap across E_F has been confirmed in both RT- and MI-type Al–Mg–Pd QCs. We propose also that the effective carrier concentration derived from the Hall coefficient may be used as a universal parameter for both RT- and MI-type QCs in place of the conventionally used electron concentration per atom. We found that the resistivity and electronic specific-heat data exhibit universal relationships when plotted as a function of the effective carrier concentration. From this we conclude that either electrons or holes dominate at E_F in most RT- and MI-type QCs studied so far. Exceptions to this will be those whose Hall coefficient is extremely small and changes its sign with temperature.

1. Introduction

Icosahedral quasi-crystals (QCs) can be grouped into two different families, depending on the building blocks of atomic clusters: one the rhombic triacontahedron (RT) type of QC, which possesses the $Mg_{32}(Al, Zn)_{49}$ Frank–Kasper compound as its $(\frac{1}{1}\frac{1}{1}\frac{1}{1})$ approximant (abbreviated to the 1/1 approximant) (Henley and Elser 1986) and the other the Mackay icosahedron (MI) type of QC having the α-phase Al–Mn–Si structure as the 1/1 approximant (Elser and Henley 1985). The RT- and MI-type QCs can be formed by liquid quenching in the Al–Mg–Pd systems. The RT-type QCs have been exclusively synthesized so far in the

0953-8984/94/367335+16$19.50

systems consisting of only simple elements such as Al, Mg, Zn, Li and Ga including the noble metals Cu and Ag. In contrast, the transition-metal elements such as Mn, Fe and Ru are involved as one of the major components in the MI-type QCs. Recently, Koshikawa *et al* (1993) revealed that both RT-and MI-type QCs can be formed by liquid quenching in the Al–Mg–Pd system. The RT-type QC was formed in the range 12–15 at.% Pd, 42–50 at.% Al and 45–53 at% Mg, whereas the MI type in the vicinity of 30 at.% Pd and 52 at.% Al.

The discussion on the pseudo-gap formation near the Fermi level E_F in the thermally stable QC and approximant is of significant importance. Its presence in the approximant has been proved theoretically (Fujiwara 1989, Fujiwara *et al* 1993, Hafner and Krajci 1993). Spectroscopic measurements have also provided ample evidence for its presence in both RT- and MI-type QCs (Belin and Traverse 1991, Matubara *et al* 1992, Mori *et al* 1991, Mizutani *et al* 1993a). A small electronic specific-heat coefficient relative to the corresponding free-electron value has also been taken as evidence of this (Kimura *et al* 1989, Biggs *et al* 1991, Mizutani *et al* 1990a, b Poon 1992). Because of the presence of the pseudo-gap at E_F, the thermally stable QCs exhibit extremely high resistivities: 10000 $\mu\Omega$ cm at 4.2 K for $Al_{70.5}Mn_{7.5}Pd_{22}$ (Lanco *et al* 1992), 6600 $\mu\Omega$ cm for $Al_{62}Fe_{12.5}Cu_{25.5}$ (Klein *et al* 1992), 10000 $\mu\Omega$ cm for $Al_{70}Cu_{15}Ru_{15}$ (Biggs *et al* 1991) and 1 Ω cm for $Al_{70}Re_{10}Pd_{20}$ (Pierce *et al* 1993).

Such unique electron transport properties should originate from the band structure involving the pseudo-gap near E_F. Belin *et al* (1993b) observed a shift in the Al 3p spectrum (valence band→Al 1s) towards high binding energies (BEs) from E_F more significant in the Al–Mn–Si 1/1 approximant having a resistivity exceeding 1000 $\mu\Omega$ cm at 300 K than the corresponding metastable QC with a resistivity of only several hundred microohm centimetres. They related the possession of a higher resistivity in the 1/1 approximant to a larger displacement of the edge of the Al 3p electron distribution towards a higher BE. In the present work we have studied systematically the electronic structure and electron transport properties of various QCs in both RT-type (including its 1/1 approximant) and MI-type families: Al–Mg–Pd, Al–Mg–Zn and Al–Mg–Cu as the former and Al–Mg–Pd, Al–Ru–Cu and Al–Re–Pd as the latter. Our objective is to extract the essential features and the characteristic difference in the electronic structure between the RT- and MI-type QCs and to discuss its effect on the electron transport properties.

2. Experimental procedure

The purities of the source metals are as follows: Al, 99.999%; Mg, 99.99%; Zn, 99.999%; Cu, 99.99%; Ru, 99.99%; Re, 99.99%, Pd, 99.99%. Arc melting or induction melting or a combination of these two was used to prepare the ingots with desired compositions. For example, the Al–Pd mother ingot was prepared by arc melting. The ternary alloy ingot was obtained by induction melting appropriate amounts of pure Mg and the Al–Pd mother alloy. A single-roll spinning-wheel apparatus with a roll diameter of 20 cm was employed to form quasi-crystalline ribbon samples. Its spinning speed was generally 5000 rev min^{-1}. The structure was examined by x-ray diffraction with Cu Kα radiation. The RT-type QCs employed in this experiment were $Al_{15}Mg_{45}Zn_{40}$, $Al_{51.9}Mg_{39.5}Cu_{8.6}$, $Al_{42}Mg_{44}Pd_{14}$ and $Al_{50}Mg_{36}Pd_{14}$, whereas the MI-type QCs were $Al_{52.5}Mg_{20}Pd_{27.5}$, $Al_{52}Mg_{18}Pd_{30}$, $Al_{61.5}Ru_{13.5}Cu_{25}$ and $Al_{70}Re_{10}Pd_{20}$. The $Al_{51.9}Mg_{39.5}Cu_{8.6}$ QC was transformed into the 1/1 approximant by heat treatment.

The electrical resistivity was measured in the range 2–760 K and the low-temperature specific heats in the range 1.6–6 K. The resistivities at 300 K for the MI-type $Al_{52}Mg_{18}Pd_{30}$, $Al_{61.5}Ru_{13.5}Cu_{25}$ and $Al_{70}Re_{10}Pd_{20}$ QCs turned out to be 700 $\mu\Omega$ cm, 1600 $\mu\Omega$ cm and

2000 $\mu\Omega$ cm, respectively. The values for the latter two QCs are smaller than those reported earlier (Biggs *et al* 1991, Pierce *et al* 1993). The Hall coefficient was measured for the RT- and MI-type Al–Mg–Pd QCs in the range 77–300 K with the use of the five-probe DC method. The x-ray photoemission valence band spectra were measured using an Al-Kα monochromated x-ray beam (Surface Science Instrument, X-probe). The Al Kβ (Al 3p distribution; valence band$\rightarrow$1s) soft-x-ray emissions were measured in both Nagoya (Japan) and Paris (France) as well as the Pd L$\beta_{2,15}$ (valence band$\rightarrow$Pd 2p$_{3/2}$) spectra for both RT- and MI-type Al–Mg–Pd QCs. The x-ray photoemission spectroscopy (XPS) and soft-x-ray spectroscopy (SXS) experiments were carried out with vacuum bent-crystal spectrometers fitted to SiO_2 1010 plates and using incoming electrons at 5 keV. The Al p conduction states (conduction states$\rightarrow$1s) were studied by the photoyield technique at the synchrotron facility, LURE, Orsay (France). The energy resolution in all these measurements was about 0.3 eV. The energy scale relative to E_F in the soft-x-ray spectra is determined within $\pm$0.2 eV by measuring the BEs of the Al 2p$_{3/2}$ and Pd 3d core levels and also the Al Kα (2p$_{3/2}\rightarrow$1s) and Pd Lα (3d$\rightarrow$2p) emission lines.

3. Results and discussion

3.1. Electron transport properties in Al–Mg–Pd QCs

The data for the electrical resistivities and the electronic specific-heat coefficients of the RT-type Al–Mg–Pd QCs have been reported elsewhere (Hashimoto *et al* 1993). Briefly, as-quenched $Al_xMg_{86-x}Pd_{14}$ (x = 42, 46, 50 and 54) samples turned out to be RT-type QCs. The samples with x = 42 and 46 were thermally stable up to the melting point, while those with x = 50 and 54 transformed into the Frank–Kasper type 1/1 approximant. The resistivity at 300 K for the thermally stable RT-type QCs after annealing is about 220 $\mu\Omega$ cm, whereas that for the 1/1 approximant is also 220 $\mu\Omega$ cm.

Both the $Al_{52.5}Mg_{20}Pd_{27.5}$ and the $Al_{52}Mg_{18}Pd_{30}$ samples can be amorphized when the rotation of the spinning wheel is increased to 6000 rev min^{-1}. Figure 1(a) shows the temperature dependence of the resistivity for the as-quenched amorphous $Al_{52}Mg_{18}Pd_{30}$ sample, the resistivity of which is 185 $\mu\Omega$ cm at 300 K. The resistivity jumps sharply at about 580 K and then rapidly decreases above 650 K. The decrease in resistivity at 650 K is due to crystallization. When the heating is terminated immediately after a jump at 580 K, as shown in figure 1(b), all diffraction lines can be indexed in terms of the MI-type QC. The resistivity at 300 K reaches 700 $\mu\Omega$ cm after heating. Hence, we took this value for the resistivity of the MI-type QC, as listed in table 1. Rather broad x-ray diffraction peaks even after heating are consistent with the fact that the QC is metastable. However, it is noted that the resistivity in the metastable MI-type QC is 3.2 times as large as that in the thermally stable RT-type QC in the Al–Mg–Pd system.

The value of γ for the MI-type $Al_{52}Mg_{18}Pd_{30}$ QC turns out to be 0.43 mJ mol^{-1} K^{-2} while that for the thermally stable RT-type QC is 0.6–0.7 mJ mol^{-1} K^{-2}. The values in both cases are relatively low but not as small as 0.1–0.3 mJ mol^{-1} K^{-2} observed in the thermally stable QCs. This indicates that the pseudo-gap exists at E_F but is relatively shallow in both QCs. The temperature dependence of the Hall coefficient is shown in figure 2 for both RT- and MI-type Al–Mg–Pd QCs. It is found that the MI-type $Al_{52}Mg_{18}Pd_{30}$ QC exhibits a positive Hall coefficient in contrast with a negative Hall coefficient for the RT-type QC. It should also be mentioned that the Hall coefficient for the other MI-type QC, $Al_{52.5}Mg_{20}Pd_{27.5}$ turned out to be negative, as listed in table 1. Hence, the sign of the Hall coefficient is very sensitive to the Pd content in this system. Indeed, Lindqvist *et al* (1993) reported that only

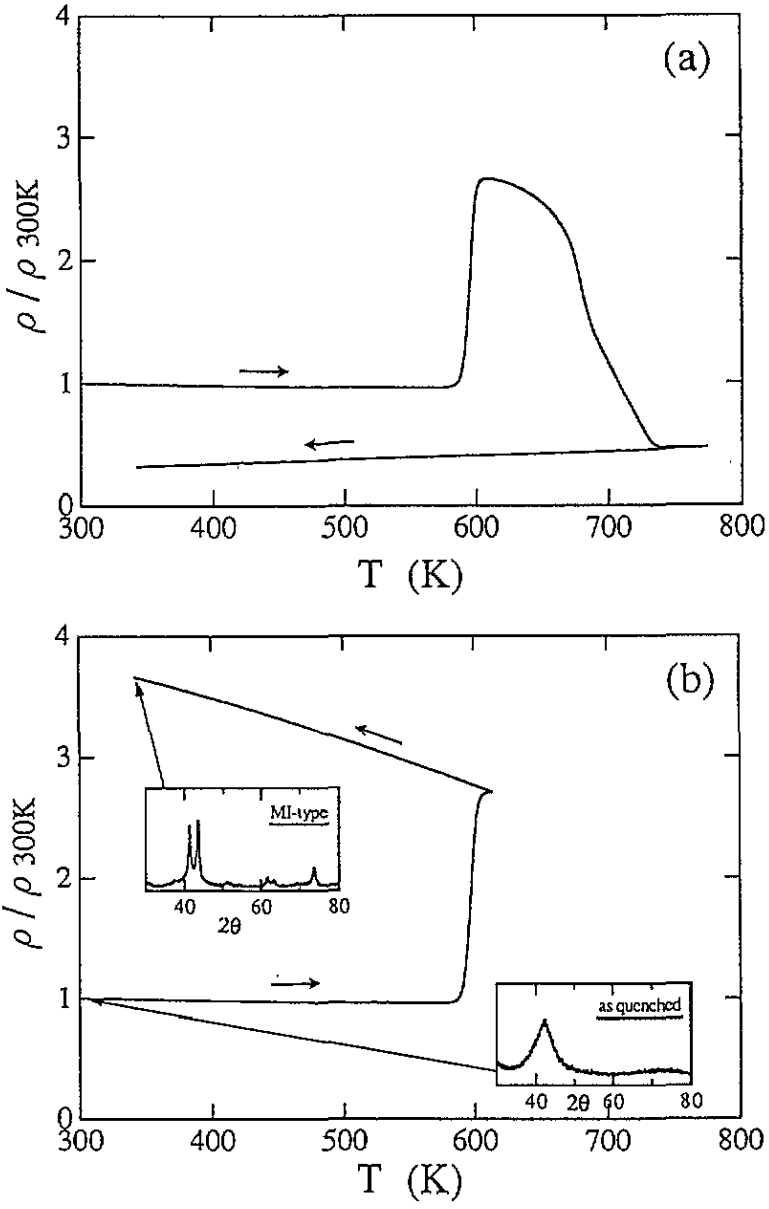

Figure 1. Temperature dependence of the electrical resistivity for the as-quenched amorphous $Al_{52}Mg_{18}Pd_{30}$ alloy. The heating rate was 10 K min^{-1}. The resistivity is normalized with respect to that at 300 K (ρ_{300K} = 185 $\mu\Omega$ cm). (a) It drops sharply above 650 K owing to crystallization. (b) The MI-type QC can be achieved when the heating is terminated at 580 K.

1% change in Fe content is large enough to cause a change in the sign of the Hall coefficient in the Al–Cu–Fe QCs. The relevant numerical data obtained for the MI-type Al–Mg–Pd QCs are summarized in table 1.

3.2. Valence band structures of MI- and RT-type Al–Mg–Pd QCs

In this section, we discuss the valence band structures in these two QCs. The x-ray

Table 1. Electronic properties of the MI-type Al–Mg–Pd QCs. The low-temperature specific-heat data are fitted to the equation $C = \gamma T + \alpha T^3 + \delta T^5$. The Debye temperature Θ_D is calculated from the equation $\Theta_D = (12\pi^4 R/5\alpha)^{1/3}$, where R is the gas constant. The electron concentration e/a is calculated by assuming that Al, Mg and Pd donate to the free-electron band 3, 2 and −0.6 electrons per atom, respectively. The value of γ_F represents the electronic specific-heat coefficient derived from the free-electron model. Note that the Hall coefficient at 300 K is positive for the 30 at.% Pd sample, but negative for the 27.5 at.% Pd sample.

Sample	γ (mJ mol^{-1} K^{-2})	α (mJ mol^{-1} K^{-4})	Θ_D (K)	δ (10^{-4} mJ mol^{-1} K^{-6})	γ_F (mJ mol^{-1} K^{-2})	ρ_{300K} ($\mu\Omega$ cm)	R_H (10^{-11} m^3 A^{-1} s^{-1})	e/a	d (g cm^{-3})
$Al_{52}Mg_{18}Pd_{30}$ annealed	0.43 ± 0.02	0.023 ± 0.002	436 ± 13	1.0 ± 0.5	0.760	700 ± 13	23.2 ± 1.6	1.74	5.02
$Al_{52.5}Mg_{20}Pd_{27.5}$ annealed	0.65 ± 0.02	0.034 ± 0.02	386 ± 7	0.7 ± 0.5	0.758	550 ± 37	-6.6 ± 0.3	1.81	4.94

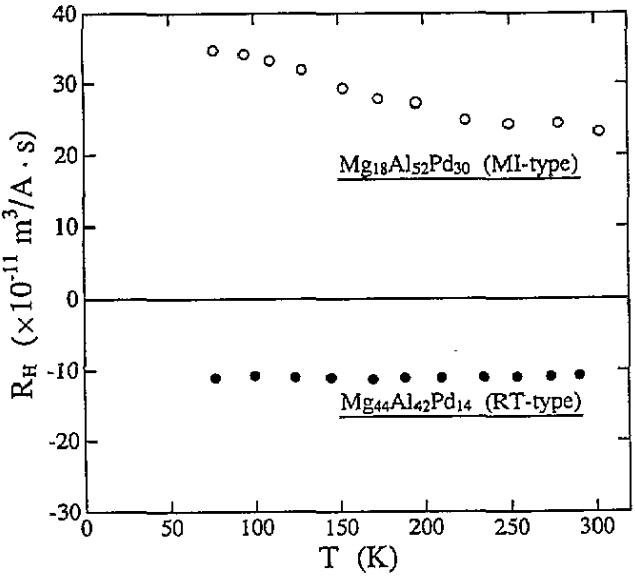

Figure 2. Temperature dependence of the Hall coefficient for the RT-type $Al_{42}Mg_{44}Pd_{14}$ and the MI-type $Al_{52}Mg_{18}Pd_{30}$ QCs. The values of R_H at 300 K for the RT-type $Al_xMg_{86-x}Pd_{14}$ (x = 42 and 46) are -10.8×10^{-11} m^3 A^{-1} s^{-1} and -15.9×10^{-11} m^3 A^{-1} s^{-1}, respectively. The values for the MI-type QCs are listed in table 1.

photoelectron valence band spectra for the RT-type $Al_{50}Mg_{36}Pd_{14}$ and MI-type $Al_{52}Mg_{18}Pd_{30}$ QCs are shown in figure 3 together with the data for the $Al_{50}Mg_{20}Pd_{30}$ sample having the CsCl-type B2 structure, which was obtained by mechanical alloying as the metastable powder form. Fuggle *et al* (1982) reported a large number of the x-ray photoelectron valence band and core level spectra for Ni- and Pd-based crystalline alloys. Among their data, the x-ray photoelectron valence band spectrum for the B2-type AlPd compound together with the corresponding band calculations is incorporated in figure 3. The present spectrum for the B2-type Al–Mg–Pd compound resembles that of the B2-type AlPd compound. The band calculations for the B2-type AlPd compound clearly show that the Pd d states are split into three major peaks centred at 1, 3.5 and 5.5 eV while the Al 3s states are centred at 7 eV below E_F. Evidently, the x-ray photoelectron valence band spectra resemble the band calculations well, not only for the B2-type Al–Mg–Pd compound but also for the MI-type QC.

Figure 4 shows both Pd L$\beta_{2,15}$ and Al Kβ emission soft-x-ray spectra for the MI- and RT-type QCs, both being normalized to the maximum intensity. The Pd L$\beta_{2,15}$ spectrum, which mainly represents the Pd 4d electron distribution, is characterized by a central peak with three weak humps labelled A, B and C in the figure. Admittedly, hump B is less clear but its presence can be traced as an asymmetric bulge of the central peak in the MI-type QC. The central peaks are located at 3.7 ± 0.4 eV and 4.1 ± 0.4 eV for the RT- and MI-type QCs, respectively. It is more important that the humps A and B coincide in position with the double peak in the Al Kβ spectrum and that the Pd 4d central peak coincides with the Al Kβ minimum in both types of QC. The Al Kβ spectrum is known to reflect the Al 3p partial density of states. Hence, we realize that the Al 3p states are depleted in the middle of the valence band and give rise to a double-peak structure.

The position of the Al Kβ double peak as well as that of the Pd L$\beta_{2,15}$ humps A and B in the MI-type QC is found to agree well with the humps in the x-ray photoelectron spectra at the BEs of 1 and 5 eV shown in figure 3. The XPS hump is visible only in the MI-type QC, being well consistent with the situation in the soft-x-ray spectra. From all these facts we conclude that both the XPS humps and the Al Kβ double peaks arise from the same origin and represent the formation of the bonding and antibonding states caused by the interaction

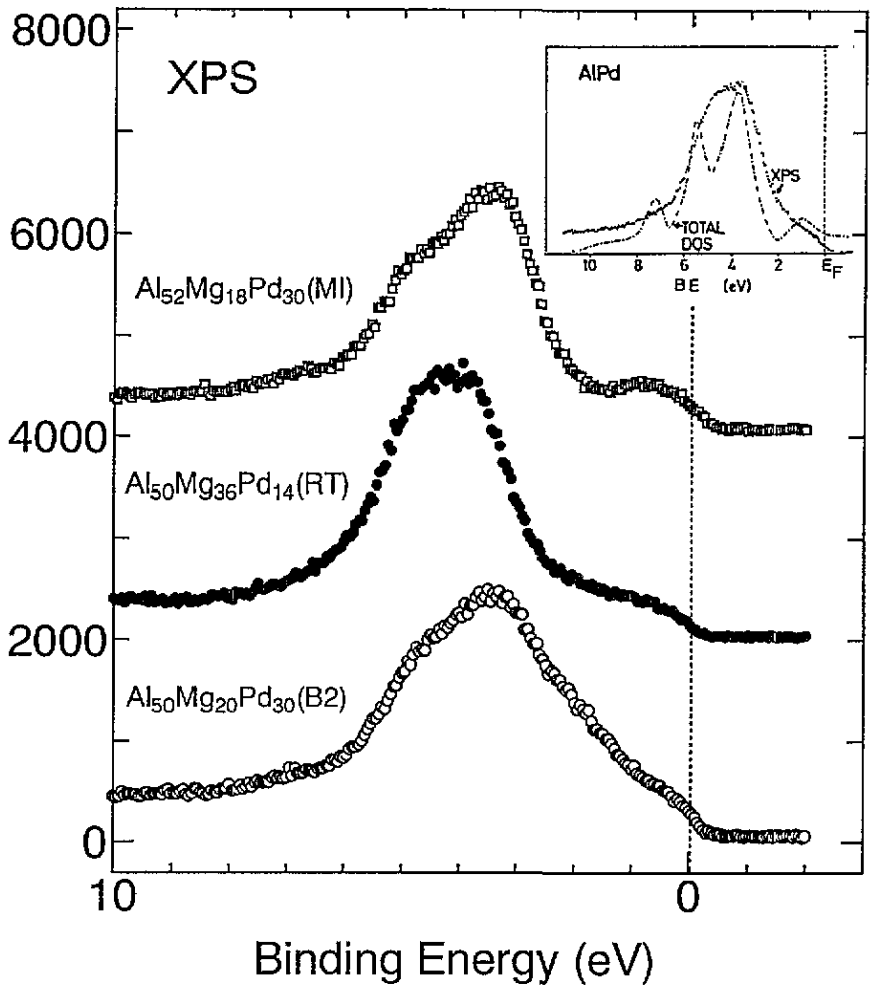

Figure 3. The X-ray photoelectron valence band spectra for the MI-type $Al_{52}Mg_{18}Pd_{30}$ QC, the RT-type $Al_{50}Mg_{36}Pd_{14}$ QC and the $Al_{45}Mg_{20}Pd_{35}$ B2 compound. The inset shows the x-ray photoelectron valence band spectrum superimposed onto the calculated density of states for the AlPd B2 compound. The data in the inset are reproduced from the work by Fuggle *et al* (1982).

of the Pd 4d states with the Al 3p states in the Al–Pd nearest-neigbour pairs. The Al 3d states may also contribute to the formation of the antibonding states at the BE of 1 eV (Dankhazi *et al* 1993).

A very faint hump at the BE of 6 eV labelled C in figure 4 reflects the Pd 4d states hybridized with Al 3s states (Belin and Dankhazi 1993). The density of states at E_F relative to that of pure Al for both MI- and RT-type QCs may be evaluated by taking the ratio of the respective SXS intensities. This ratio turned out to be 47/50 and 41/50 for the MI- and RT-type QCs, respectively. Hence, more Al 3p electrons should be pushed towards E_F, resulting in a higher Al 3p density of states at E_F in the MI- than in the RT-type QCs.

Figure 5 shows the conduction (absorption) Al p state distribution for both types of QC, together with that of pure Al (full circles) shown as a reference. For convenience, the Al Kβ emission spectra shown in figure 4 are superimposed. The absorption spectra are normalized to the intensity value at E_F taken equal to that of the Al Kβ emission band

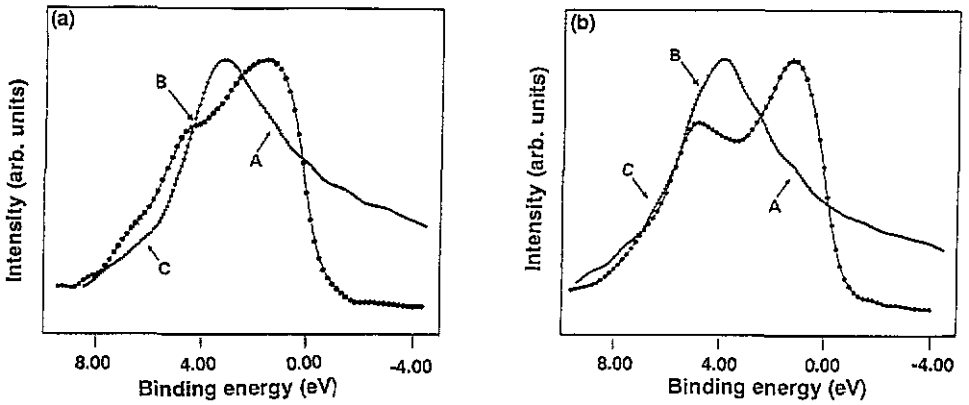

Figure 4. The Al Kβ (●) and Pd L$\beta_{2,15}$ (*) emission soft-x-ray spectra for (a) RT-type $Al_{50}Mg_{36}Pd_{14}$ and (b) MI-type $Al_{52}Mg_{18}Pd_{30}$ QCs. The origin of the scale is set to the Fermi level. A, B and C indicate the humps on the Pd L$\beta_{2,15}$ spectra.

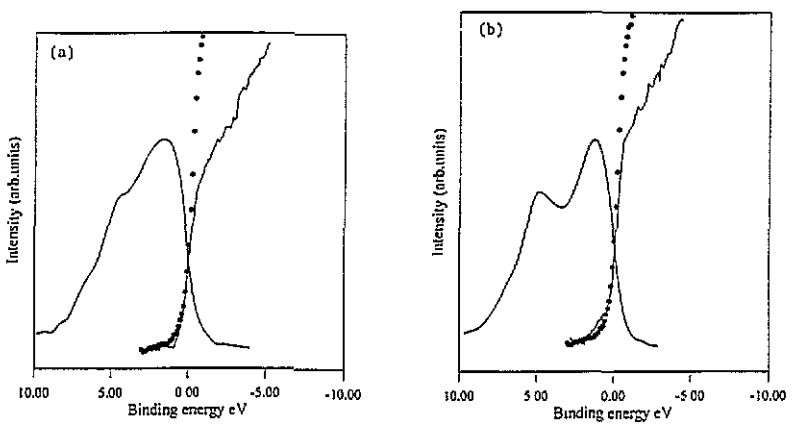

Figure 5. The Al p conduction band spectra for (a) the RT-type $Al_{50}Mg_{36}Pd_{14}$ and (b) the MI-type $Al_{52}Mg_{18}Pd_{30}$ QCs: ●, data for pure Al as a reference. Also the Al Kβ emission spectra shown in figure 4 are shown for comparison. The origin of the scale is set to the Fermi level. The intensities of both emission and absorption spectra are normalized to unity at the Fermi level.

spectra. By comparison with the absorption data for pure Al, we realize that there is a small depopulation of the Al conduction band states in both types of QC. This small decrease in Al conduction states is involved in the formation of the pseudo-gap. Note that they are much less significant than those observed in the thermally stable Al–Cu–Fe and Al–Pd–Mn (Belin *et al* 1993a), suggesting that the pseudo-gap in the present QCs is rather shallow. This is consistent with the electronic specific-heat coefficient discussed in section 3.1.

3.3. Valence band structures in MI- and RT-type QCs

Figures 6(a) and 6(b) show the x-ray photoelectron and Al Kβ soft-x-ray spectra for the RT-type QCs and figures 6(c) and 6(d) the corresponding spectra for the MI-type QCs. The Al–Mg–Pd data discussed in section 3.2 are also incorporated. The data for the Al–Mg–Cu system were taken from the 1/1 approximant sample obtained by annealing the metastable

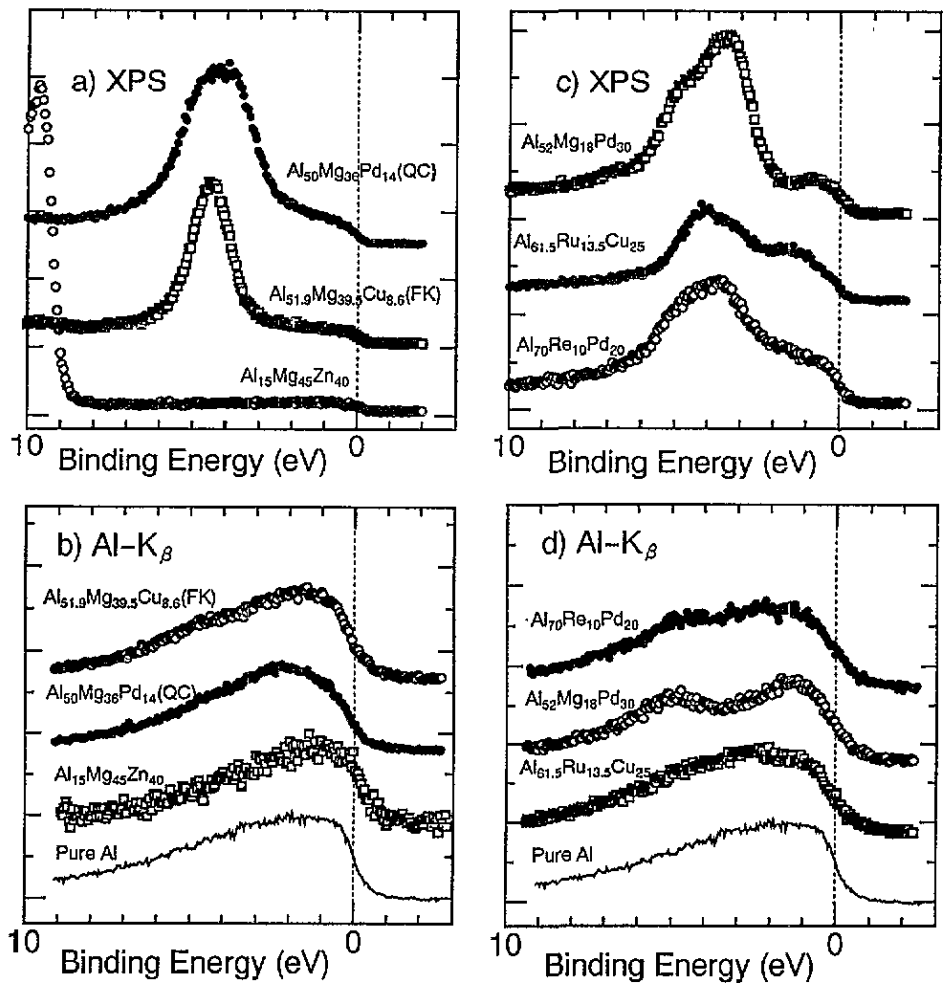

Figure 6. (a) The x-ray photoelectron valence band spectra and (b) the Al Kβ soft-x-ray emission band spectra for the RT-type $Al_{15}Mg_{45}Zn_{40}$ QC, the 1/1 approximant $Al_{51.9}Mg_{39.5}Cu_{8.6}$ and the RT-type $Al_{50}Mg_{36}Pd_{14}$ QC; (c) the x-ray photoelectron valence band spectra and (d) the Al Kβ soft-x-ray emission band spectra for the MI-type $Al_{52}Mg_{18}Pd_{30}$, $Al_{61.5}Ru_{13.5}Cu_{25}$ and $Al_{70}Re_{10}Pd_{20}$ QCs. The soft-x-ray spectrum for pure Al is also shown for comparison.

QC above its crystallization temperature of 530 K. No measurable difference was found in the XPS valence band structure between the metastable RT-type QC and its 1/1 approximant (Hashimoto *et al* 1993). Hence we shall ignore any difference between their valence band structures in the following discussion.

We start our discussions with the valence band structure for the MI-type QCs. Relative to those for the RT-type QCs, a definite enhancement in the XPS intensities has been observed in the BE range 0–2 eV for all three MI-type QCs. It has been well known that the d states of the early-transition metals (ETs) appear at lower BEs than those of the late-transition metals (LTs) in the ET–LT type of alloys. Hence, the enhancement in the range 0–2 eV in the Al–Ru–Cu and Al–Re–Pd QCs can be attributed to the d states associated with the ETs Ru and Re. In the case of the MI-type Al–Mg–Pd QC, no ET is involved but the hump is still seen at a BE of 1 eV. This was attributed to the interaction of Pd 4d states with Al (and

possibly Mg) 3p and 3d states.

As another prominent feature in the XPS valence band of the MI-type QCs, we can point out the broadness of the main peak relative to that of the RT-type QCs. The peaks are located at a BE of 3–5 eV and are easily identified as the Pd 4d (or Cu 3d) states for the Al–Mg–Pd, Al–Ru–Cu and Al–Re–Pd QCs. It can be seen that all soft-x-ray spectra in the MI-type QCs exhibit a minimum at a BE of aboue 3.5–4 eV, the position being in good agreement with the XPS main peak mentioned above. As discussed in the preceding section, this is caused by the depletion of the Al 3p states due to their interaction with the Pd 4d (or Cu 3d) states in this energy range.

An increasing Pd 4d–Al 3p hybridization effect accelerates the formation of the bonding and antibonding states, resulting in a deeper minimum in the Al 3p electron distribution. The Pd–Al antibonding states formed immediately below E_F cannot be widely spread but should be confined in the energy range 0–3 eV because of the presence of the pseudo-gap near E_F. This would act to flatten the energy dispersion for the Al 3p electrons and to enhance the density of states and effective mass in this energy range. Then one would naturally think that a larger enhancement of the Al 3p distribution immediately below E_F would lead to a high electrical resistivity. As mentioned in the introduction, the resistivity value at 300 K for all MI-type QCs is indeed very high in comparison with those for the RT-type QCs. However, the situation may not be so simple. Of the three MI-type QCs shown in figure 6, the enhancement in the Al Kβ spectra in the range 0–3 eV is the largest for the Al–Mg–Pd but is rather less significant for Al–Ru–Cu and Al–Re–Pd, the latter two possessing resistivities higher than that of Al–Mg–Pd. This is because the Al 3p electrons in the Al–Re–Pd and Al–Ru–Cu QCs interact with the d states associated with the ETs Re and Ru in this energy range and the dispersionless E–k relation originating from these d states also affects the Al 3p distributions and contributes further to a large enhancement in resistivity.

The x-ray photoelectron valence band spectra for the RT-type Al–Mg–Zn, Al–Mg–Cu and Al–Mg–Pd QCs or the 1/1 approximant are characterized by the possession of a rather sharp main peak associated with the Pd or Cu d states. The Zn 3d band is also seen at the bottom of the valence band. The sharp peak implies that the transition-metal atoms Cu and Pd are distributed in as isolated a manner as possible in the matrix. The valence band structure towards E_F is quite flat or slightly declining without any noticeable hump. This indicates that the d states associated with transition metals are essentially negligible at E_F. The Al Kβ spectra in the RT-type QCs resemble that of pure Al, although a double-peak structure is still weakly seen in Al–Mg–Cu and Al–Mg–Pd. The lack of a sizable double-peak structure suggests that the probability of having the Al–Pd nearest-neighbour pair is much lower than in the MI-type QCs. Thus, the Al atom serves as a metal element donating free electrons to the valence band. This means that the free-electron picture may be used to describe the electronic structure in the RT-type QCs as well as their 1/1 approximants, regardless of the Al concentration and partner elements involved.

It is of interest, at this stage, to compare the Al 3p electron distribution in the RT- and MI-type QCs with that in Al-based amorphous Al–ET–LT (ET ≡ Ti, Y, Zr or La; LT ≡ Ni or Cu) alloys (Mizutani *et al* 1993b). As a typical example, the Al Kβ emission spectra for the amorphous $Al_{30}Y_{42}Cu_{28}$ and $Al_{85}Y_9Cu_6$ alloys are shown in figure 7. The Al 3p electrons are almost fully immersed below E_F in the amorphous $Al_{30}Y_{42}Cu_{28}$ alloy whose resistivity at 300 K reaches 252 $\mu\Omega$ cm. Here the Al atom acts as a metalloid element like B and Si in the sense that the Al–Al nearest-neighbour pair is scarcely formed. Instead, Al atoms preferentially form the bonding and/or antibonding states with the neighbouring Cu and Y metals, resulting in the disappearance of the Al 3p electrons at E_F. Nevertheless,

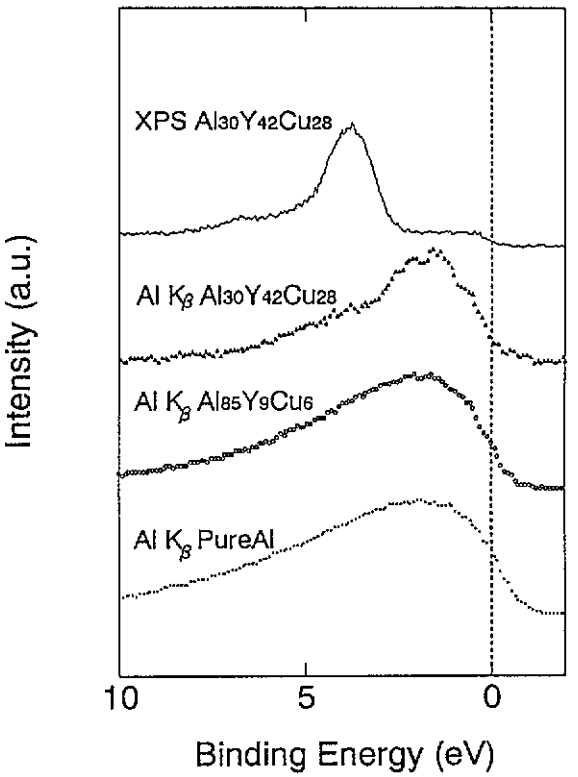

Figure 7. The Al $K\beta$ emission soft-x-ray spectrum for the amorphous $Al_{30}Y_{42}Cu_{28}$ and $Al_{85}Y_9Cu_6$ alloys (Mizutani *et al* 1993a) (a.u., arbitrary units). The data for pure Al are also shown for comparison.

the measured electronic specific-heat coefficient of 2.4 mJ mol^{-1} K^{-2} is fairly high relative to that observed in QCs, indicating no pseudo-gap formation in such amorphous alloys. Thus, the current in the Al-poor amorphous alloy should be conveyed almost exclusively by Y 4d electrons at E_F. This is responsible for the occurrence of weak-localization effects (Mizutani *et al* 1993b).

The Al atom changes its role when its concentration exceeds about 60 at.% in the amorphous matrix. As shown in figure 7, the free-electron-like spectrum is observed for the $Al_{85}Y_9Cu_6$ alloy whose resistivity is only 63 $\mu\Omega$ cm. Now all the physical properties including the x-ray photoelectron valence band spectra, the Al $K\beta$ soft-x-ray spectra, the magnitudes of the resistivity and electronic specific-heat coefficient and the sign and magnitude of the Hall coefficient become consistent with the free-electron behaviour (Mizutani *et al* 1993b). A comparison of the Al $K\beta$ spectra in figures 6(d) and 7 leads us to realize that the Al 3p density of states at E_F in the amorphous $Al_{30}Y_{42}Cu_{28}$ alloy is much smaller than in the QCs, despite the fact that its resistivity of 250 $\mu\Omega$ cm is significantly lower than observed in the thermally stable MI-type QCs. Therefore, we conclude that information about the Al 3p distribution at E_F is important but it is not the only parameter to explain the origin for the occurrence of extremely high resistivities observed in a number of thermally stable QCs containing more than 50 at.% Al. Investigation of both valence and conduction electronic distributions of all the elements of each given alloy, using a combination of various techniques such as XPS, SXS and electronic specific-heat coefficient measurements, should be necessary to describe totally the density of states and to discuss completely the electronic interactions between Al and the other components.

3.4. Electronic specific-heat coefficient in MI- and RT-type QCs

In the preceding section, we emphasized that the presence of the pseudo-gap near E_F is a characteristic feature in QCs and gives rise to their unique electron transport properties. Admittedly, however, the depth of the pseudo-gap at E_F cannot be quantitatively evaluated from the measured x-ray photoelectron and/or soft-x-ray spectra. The electronic specific-heat coefficient γ, instead, would provide more straightforward information at E_F. The measured values of γ are plotted in figure 8 as a function of the electron concentration for both MI- and RT-type QCs. The electron concentration is calculated by assuming the nominal valencies for constituent elements such as Al and Mg. However, the valency for transition metals is less clear. The valency of Pd is reasonably assumed to be 0 in the case of RT-type QCs (Takeuchi *et al* 1993) but may be better chosen as -0.6 in the case of MI-type QCs (Mizutani *et al* 1993a). When this is done, a whole set of data for the RT- and MI-type QCs apparently constitutes respective universal curves, as shown in figure 8; the RT-type QC appears in the range $e/a > 2.0$ while the MI-type QC is in the range $e/a < 2.0$. Regardless of the atomic species involved, the value of γ for the RT-type QCs decreases with decreasing e/a and is extrapolated to zero at about $e/a = 2.0$. It is true that the thermally stable RT-type QCs appear in the range $2.05 < e/a < 2.2$ and always possess the smallest value of γ. The resistivity behaves inversely; it increases in proportion to a decrease in γ. A minimum value of γ so far found in this family is 0.32 mJ mol^{-1} K^{-2} in the Al–Li–Cu QC, which accompanies the maximum resistivity of 870 $\mu\Omega$ cm (Kimura *et al* 1989). Hence, there is a clear inverse relationship between the resistivity value and the electronic specific-heat coefficient in the RT-type QCs.

The value of γ for the family of the MI-type QCs also shows a clear e/a dependence and takes small but finite values in the neighbourhood of $e/a = 1.8$. Here the lowest value of γ is 0.11 mJ mol^{-1} K^{-2} observed for the thermally stable Al–Ru–Cu QC (Biggs *et al* 1991). Indeed, the resistivity is known to take extremely high values in the corresponding QCs. However, it should be noted that the highest resistivity reaching 1 Ω cm at low temperatures has been reported to occur in the thermally stable $Al_{70}Re_{10}Pd_{20}$ QC but to accompany a value of γ of 0.22 mJ mol^{-1} K^{-2} (Pierce *et al* 1993). The resistivity in non-periodic systems such as the thermally stable QCs, in which the mean free path is already constrained by an average atomic distance, is determined not only by the number of electrons at E_F but also by their effective mass calculated from the energy dispersion curve. The latter depends on the details of the density of states at E_F. Indeed, the formation of the energy gap is suggested from the measured optical conductivity data in the Al–Re–Pd QCs (Basov *et al* 1993).

Before ending this section, we emphasize the fact that the electron concentration is not a well defined parameter to describe the electron transport universally for both RT- and MI-type QCs. As we have done in constructing figure 8, negative valencies are conventionally assigned for transition metals such as Pd without rigorous physical reasoning. This difficulty has recently been pointed out by Lindqvist *et al* (1993). They noted that the Hall coefficient changes its sign when the resistivity becomes extremely high in the Al–Cu–Fe QCs. In the next section, we attempt to plot the electronic specific-heat coefficient and the resistivity at 300 K as a function of the carrier concentration deduced from the Hall coefficient for both RT- and MI-type QCs and we show that the carrier concentration thus obtained serves as a better parameter than e/a to discuss the electron transport universally for both RT- and MI-type QCs.

3.5. Hall coefficient in MI- and RT-type QCs

Many investigators have frequently evaluated the effective carrier concentration n for QCs

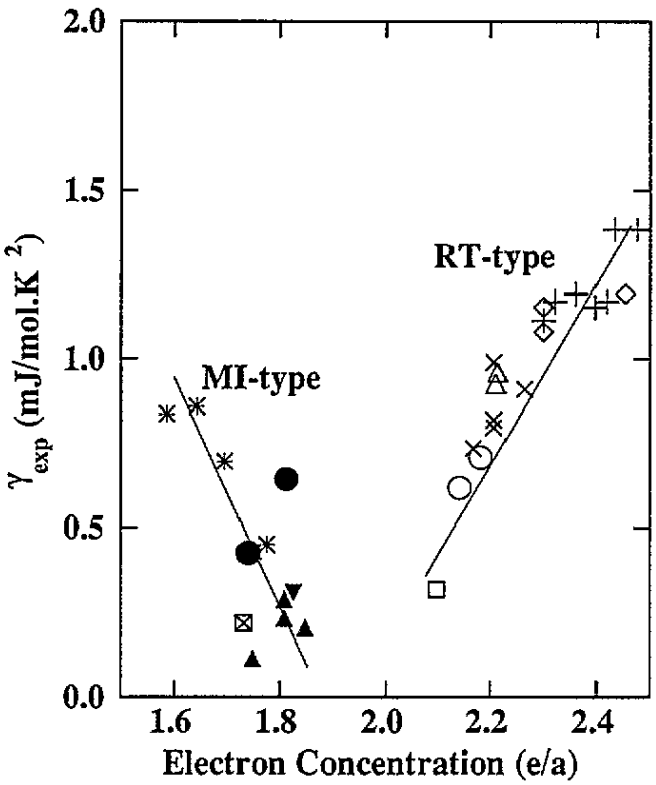

Figure 8. Electron concentration dependence of the measured electronic specific-heat coefficient in both RT-type QCs (+, Al–Mg–Cu (Mizutani *et al* 1990a, b, 1991a); ◇, Al–Mg–Ag (Mizutani *et al* 1990a, b, 1991a); △, Al–Mg–Zn (Mizutani *et al* 1991a); ×, Mg–Zn–Ga (Mizutani *et al* 1990a, b, 1991a); □, Al–Li–Cu (Kimura *et al* 1989); ○, Al–Mg–Pd (Hashimoto *et al* 1993)) and MI-type QCs (▲, Al–Ru–Cu (Mizutani *et al* 1990a, b, Biggs *et al* 1991); ▼, Al–Fe–Cu (Poon 1992); ⊠, Al–Re–Pd (Pierce *et al* 1993); ●, Al–Mg–Pd (Hashimoto *et al* 1993)). The data for the Al–Co–Ni decogonal QCs (*) are also included (Mizutani *et al* 1993a).

and approximants from the measured Hall coefficient R_H at 300 K through the equation

$$R_H = \frac{1}{ne} \tag{1}$$

where the electronic charge e is negative for electrons and positive for holes and n is the carrier concentration per cubic centimetre. However, the Fermi surfaces of electrons and holes would coexist in QCs and approximants. The Hall coefficient in the presence of two carriers is expressed at low magnetic fields as

$$R_H = \frac{\sigma_e^2 R_e + \sigma_h^2 R_h}{(\sigma_e + \sigma_h)^2} = \frac{n_e \mu_e^2 - n_h \mu_h^2}{e(n_e \mu_e - n_h \mu_h)^2} \tag{2}$$

where σ and μ represent the conductivity and mobility and the subscripts e and h stand for electrons and holes, respectively (Ziman 1964). Hence, the effective carrier concentration deduced from equation (1) no longer represents the total carrier concentration $n_e + n_h$ but is reduced to the difference $n_e - n_h$, if the mobilities of both electrons and holes are assumed to be equal to each other. Hence, one may say that only one of the carriers dominates at

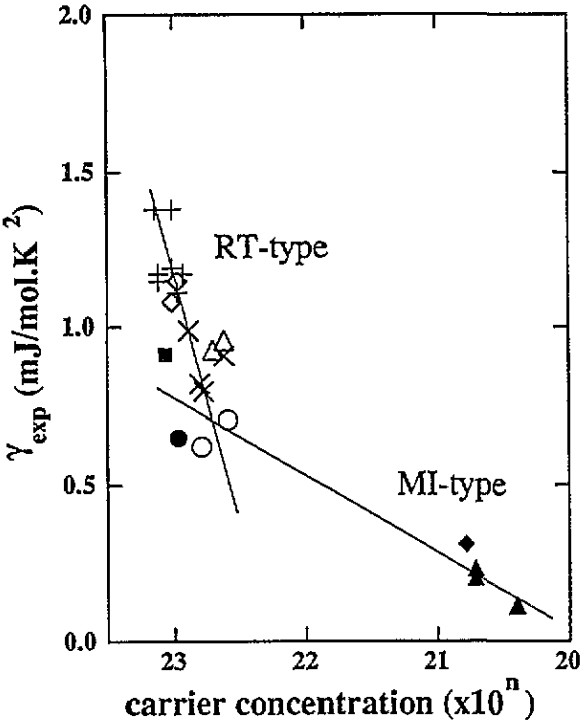

Figure 9. The electronic specific-heat coefficient γ_{exp} as a function of the effective carrier concentration for various RT- and MI-type QCs whose Hall coefficient is negative over an entire temperature range below 300 K, where the effective carrier concentration is simply calculated by inserting the measured Hall coefficient at 300 K into equation (1): ■, Al–Cu–V (Mizutani *et al* 1991b); the other symbols are the same as in figure 8.

E_F, provided that the effective carrier concentration deduced from equation (1) can be used as a universal parameter to analyse various electronic properties.

The elecrtronic specifico-heat coefficient γ_{exp} is shown in figure 9 as a function of the effective carrier concentration for both RT- and MI-type QCs. Here only the data which exhibit negative Hall coefficients are plotted with the assumption that the electron Fermi surface dominates. We can clearly see that both sets of data fall on the respective lines regardless of the atomic species involved and that the value of γ_{exp} decreases with decreasing carrier concentration. An extrapolation of the fitted lines to $\gamma_{exp} = 0$ for the RT- and MI-type QCs crosses at different carrier concentrations, indicating the presence of different zones between them.

The resistivity at 300 K is plotted in figure 10 as a function of the effective carrier concentration for RT- and MI-type QCs. The data with negative Hall coefficients are shown in figure 10(a) whereas those with positive Hall coefficients are shown in figure 10(b). The latter is assumed to have the hole Fermi surface. It can be seen that the resistivity increases with decreasing carrier concentration, irrespective of the atomic species involved. The different fitting lines are drawn through the data points for the RT- and MI-type QCs in figure 10(a). A similar line may be also drawn for the MI-type QCs in figure 10(b). The present analysis suggests that either electrons or holes apparently dominate in both types of QC and approximant shown in figures 9 and 10.

However, we must admit that there are QCs in which the two carriers most probably coexist and the electron–hole balance is very delicate. Such data would deviate from the straight line in figure 10. Lindqvist *et al* (1993) recently reported that the minimum of the conductivity and the sign reversal of the Hall coefficient occur concurrently at 12.5 at.% Fe in the stable Al–Fe–Cu QCs and suggested that the anomalous dispersion induced by the sp–d hybridization effect may be the origin of these behaviours. At the critical composition

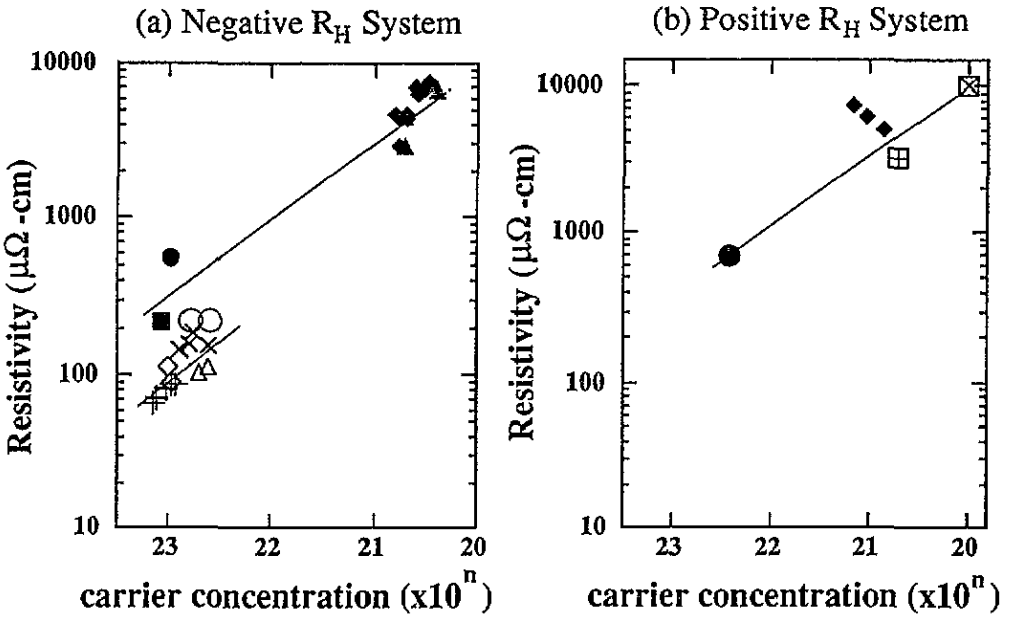

Figure 10. The resistivity at 300 K as a function of the effective carrier concentration for various RT- and MI-type QCs and approximant, where the data included are (a) those whose Hall coefficient is negative and (b) those whose Hall coefficient is positive over an entire temperature range below 300 K: ♦, Al–Fe–Cu (Lindqvist *et al* 1993); ⊞, α-phase Al–Mn–Si approximant (Poon 1992); the other symbols are the same as in figure 8.

they found that the Hall coefficient is small and changes its sign with temperature. The data reported by Lindqvist *et al* are also included in figure 10. It is seen that the data with a negative sign happened to fall on the universal line but the deviation is apparent for the data with a positive sign.

4. Conclusion

The valence band structure for the RT-type QCs and their approximants is well described by a quasi-free-electron-like monotonic density of states near E_F in the interaction at 3–5 eV with a sharp d-states peak associated with transition metals. Hence, the interaction with the d states is almost negligible at E_F. Instead, the valence band structure for the MI-type QCs consists of the d states of the LTs at higher BE and that of the ETs at lower BE. In the case of the MI-type Al–Mg–Pd QC containing no ETs, the Pd 4d states are widely spread over 0–6 eV. The Al 3p electrons are heavily depleted in the energy range where the d states of the LT is centred. This is taken as evidence for the existence of strong hybridization effects between Pd 4d and Al 3p states in the Al–Pd nearest neighbours.

The band calculations (Fujiwara *et al* 1993) tell us that the dispersionless E–k relationship originates from the folding of the zones in approximants and gives rise to a spiky density-of-states curve. We consider that the spiky peak is sharper, if both the depletion minimum in the Al 3p electron distribution and the pseudo-gap are deepened and also if the d states associated with the ET are present in the range 0–3 eV. This is the case for the MI-type QCs and is responsible for the higher resistivities.

The effective carrier concentration is calculated from the measured Hall coefficient at 300 K for both RT- and MI-type QCs. It turned out that both the electronic specific-heat coefficient and the electrical resistivity at 300 K can be well described by the carrier concentration rather than by the conventional e/a for both RT- and MI-type QCs.

References

Basov D N, Pierce F S, Volkov P, Poon S J and Timusk T 1993 *Phys. Rev. Lett.* submitted

Belin E and Dankhazi Z 1993 *J. Non-Cryst. Solids* **153–4** 298

Belin E, Dankhazi Z and Sadoc A 1993a *Proc. 8th Int. Conf. on Rapidly Quenched Materials (Sendai, 1993)*

Belin E, Miyoshi Y, Yamada Y, Ishikawa T, Matsuda T and Mizutani U 1993b *Proc. 8th Int. Conf. on Rapidly Quenched Materials (Sendai, 1993)*; 1994 *Mat. Sci. Eng.* A **181/182** 730–3

Belin E and Traverse A 1991 *J. Phys.: Condens. Matter* **3** 2157

Biggs B D, Poon S J and Munirathnam N R 1991 *Phys. Rev. Lett.* **65** 123

Dankhazi Z, Trambly de Laissardiere G, Nguyen Manh D, Belin E and Mayou D 1993 *J. Phys.: Condens. Matter* **5** 3339

Elser V and Henley C L 1985 *Phys. Rev. Lett.* **55** 2883

Fuggle J C, Ulrich Hillebrecht F, Zeller R, Zolnierek Z and Bennet P A 1982 *Phys. Rev.* B **27** 2145

Fujiwara T 1989 *Phys. Rev.* B **40** 942

Fujiwara T, Yamamoto S and Trambly de Laissardiere G 1993 *Phys. Rev. Lett.* **71** 4166

Hafner J and Krajci M 1993 *Phys. Rev.* B **47** 11 795

Hashimoto K, Yamada Y, Yamauchi T, Tanaka T, Matsuda T and Mizutani U 1993 *Proc. 8th Int. Conf. on Rapidly Quenched Materials (Sendai, 1993)*; 1994 *Mat. Sci. Eng.* A **181/182** 785–9

Henley C L and Elser V 1986 *Phil. Mag.* B **53** L59

Kimura K, Iwahashi H, Hahsimoto T, Takeuchi S, Mizutani U, Ohashi S and Itoh G 1989 *J. Phys. Soc. Japan* **58** 2472

Klein T, Rakoto H, Berger C, Fourcaudot G and Cyrot-Lackmann F 1992 *Phys. Rev.* B **45** 2046

Koshikawa N, Edagawa K and Takeuchi S 1993 *Mater. Trans. Japan Inst. Met.* **34** 188

Lanco P, Klein T, Berger C, Cyrot-Lackmann F, Fourcaudot G and Sulpice A 1992 *Europhys. Lett.* **18** 227

Lindqvist P, Berger C, Klein T, Lanco P and Cyrot-Lackmann F 1993 *Phys. Rev.* B **48** 630

Matubara H, Ogawa S, Kinoshita T, Kishi K, Takeuchi S, Kimura K and Suga S 1991 *Japan. J. Appl. Phys.* **30** L389

Mizutani U, Kamiya A, Matsuda T, Kishi K and Takeuchi S 1991a *J. Phys.: Condens. Matter* **3** 3711

Mizutani U, Kamiya A, Matsuda T and Takeuchi S 1991b *Mater. Sci. Eng.* A **133** 111

Mizutani U, Matsuda T, Itoh Y, Tanaka K, Domae H, Mizuno T, Murasaki S, Miyoshi Y, Hashimoto K and Yamada Y 1993a *J. Non. Cryst. Solids* **156–8** 882

Mizutani U, Sakabe Y and Matsuda T 1990a *J. Phys.: Condens. Matter* **2** 6153

Mizutani U, Sakabe Y, Shibuya T, Kishi K, Kimura K and Takeuchi S 1990b *J. Phys.: Condens. Matter* **2** 6169

Mizutani U, Sugiura H, Yamada Y, Sugiura Y and Matsuda T 1993b *Proc. 8th Int. Conf. on Rapidly Quenched Materials (Sendai, 1993)*; 1994 *Mat. Sci. Eng.* A **179/180** 132–6

Mori M, Matsuo S, Ishimasa T, Matsuura T, Kamiya K, Inokuchi H and Matsukawa T 1991 *J. Phys.: Condens. Matter* **3** 767

Pierce F S, Poon S J and Guo Q 1993 *Science* **261** 737

Poon S J 1992 *Adv. Phys.* **41** 303

Takeuchi T, Yamada Y, Fukunaga T and Mizutani U 1993 *Mater. Sci. Eng.* at press

Ziman J M 1964 *Principles of the Theory of Solids* (Cambridge: Cambridge University Press)